Local Clustering of Transferrin Receptors Promotes Clathrin-Coated Pit Initiation

Local clustering of transferrin receptors promotes clathrin-coated pit initiation

Allen P. Liu,[1] François Aguet,[2] Gaudenz Danuser,[2] and Sandra L. Schmid[1]

[1]Department of Cell Biology, The Scripps Research Institute, La Jolla, CA 92037
[2]Department of Cell Biology, Harvard Medical School, Boston, MA 02115

Clathrin-mediated endocytosis (CME) is the major pathway for concentrative uptake of receptors and receptor–ligand complexes (cargo). Although constitutively internalized cargos are known to accumulate into maturing clathrin-coated pits (CCPs), whether and how cargo recruitment affects the initiation and maturation of CCPs is not fully understood. Previous studies have addressed these issues by analyzing the global effects of receptor overexpression on CME or CCP dynamics. Here, we exploit a refined approach using expression of a biotinylated transferrin receptor (bTfnR) and controlling its local clustering using mono- or multivalent streptavidin. We show that local clustering of bTfnR increased CCP initiation. By tracking cargo loading in individual CCPs, we found that bTfnR clustering preceded clathrin assembly and confirmed that bTfnR-containing CCPs mature more efficiently than bTfnR-free CCPs. Although neither the clustering nor the related changes in cargo loading altered the rate of CCP maturation, bTfnR-containing CCPs exhibited significantly longer lifetimes than other CCPs within the same cell. Together these results demonstrate that cargo composition is a key source of the differential dynamics of CCPs.

Introduction

Clathrin-mediated endocytosis (CME) supports efficient internalization of ligands and their receptors (i.e., cargo) from the cell surface. During initiation of clathrin-coated pits (CCPs) and subsequent maturation, receptors are thought to be concentrated through interactions between sorting motifs in their cytoplasmic tails and adaptor proteins. As clathrin assembles, CCPs invaginate and eventually pinch off to form cargo-laden clathrin-coated vesicles (CCVs). Whether active clustering of receptors promotes CCP initiation is unclear. Furthermore, it is not well understood to what extent receptors represent passive "passengers" in CCPs or whether, and by which mechanism(s), they contribute to the regulation of the dynamic properties of CCPs (Keyel et al., 2006; Lakadamyali et al., 2006; Puthenveedu and von Zastrow, 2006). That is, must CCPs be fully loaded with cargo before they pinch off? Is the rate of CCP maturation affected by the rate or degree of cargo loading?

Several studies have shed light on how cargo molecules might affect the dynamic behavior of individual CCPs. For example, Ehrlich et al. (2004) have shown that CCP lifetimes are proportional to the size of internalized cargo particles, presumably because more clathrin triskelia are needed to form larger CCVs. However, different ligands were used (i.e., transferrin, low density lipoprotein [LDL] particles, and reoviruses) that engage different numbers and classes of receptors, which in turn use different adaptor proteins. These differences could also directly affect the kinetics of CCP maturation. Indeed, subsets of CCPs containing ligand-activated G protein–coupled receptors (GPCRs) and their specific adaptor proteins exhibited altered internalization kinetics in living cells (Puthenveedu and von Zastrow, 2006).

Recent evidence has suggested that constitutively internalized cargo receptors that use distinct adaptors can differentially affect CCP dynamics. Using live-cell imaging and computational decomposition of the CCP lifetime distribution, Loerke et al. (2009) found that overexpression of transferrin

Correspondence to Gaudenz Danuser: Gaudenz_Danuser@hms.harvard.edu; or Sandra L. Schmid: slschmid@scripps.edu

Abbreviations used in this paper: bTfnR, biotinylated transferrin receptor; CCP, clathrin-coated pit; CCV, clathrin-coated vesicle; CME, clathrin-mediated endocytosis; GPCR, G protein–coupled receptor; LCa, clathrin light chain; SA, streptavidin; Tfn, transferrin; TfnR, transferrin receptor; TIR-FM: total internal reflection fluorescence microscopy.

The Rockefeller University Press $30.00
J. Cell Biol. Vol. 191 No. 7 1381–1393
www.jcb.org/cgi/doi/10.1083/jcb.201008117

receptors (TfnRs) increased the ratio of productive to abortive CCPs without affecting their lifetimes, suggesting that cargo concentration plays a role in stabilizing nascent CCPs, i.e., by enhancing their maturation efficiency. In contrast, CCP lifetimes were increased and the fraction of productive CCPs decreased by overexpression of LDL receptors (LDLRs; Mettlen et al., 2010). Interestingly, neither overexpression of TfnR nor LDLR increased CCP density at the plasma membrane (Loerke et al., 2009; Mettlen et al., 2010).

These studies suggest that cargo molecules are not passive passengers during CME and that cargo can regulate different aspects of CCP dynamics. However, cargo overexpression under these conditions reduces the efficiency of CME, presumably by altering the availability of other limiting components (Warren et al., 1997, 1998; Loerke et al., 2009), thus rendering the interpretation of these experiments more difficult. To overcome this limitation, we developed new tools to systematically manipulate the local concentration of TfnRs, which also enabled us to directly visualize the dynamic behavior of the TfnR-laden CCPs, relative to the ensemble. Using this approach, we have examined the relationship between cargo accumulation into CCPs and the regulation of CCP initiation and maturation.

Results

Systematic manipulation of TfnR clustering

Proteomic studies have identified TfnRs as a major cargo in CCV preparations from cultured cells (Borner et al., 2006); therefore, we have chosen TfnR as a model cargo molecule for CME. The YXXΦ (YTRF) motif in the cytoplasmic tail of TfnR (Collawn et al., 1990) is recognized by the μ2 subunit of AP-2 (Ohno et al., 1995; Nesterov et al., 1999). A previous study showed that the rate of internalization of cross-linked, decameric Tfn was reduced by approximately twofold, suggesting that clustering of TfnR reduced their uptake (Marsh et al., 1995). However, the decameric Tfn used in these studies was large (Stokes radius ∼84 Å; Ikai et al., 1988). In view of the more recent finding that increased cargo size slows the internalization rate (Ehrlich et al., 2004), it is unclear whether the observation by Marsh et al. (1995) is related to the altered cargo size or the shorter distance, i.e., the clustering, of YXXΦ motifs. Therefore, we sought a new approach to manipulate the local concentration of TfnRs within CCPs, without altering either global receptor concentration or ligand size.

Recently, several methodologies have been developed to attach protein- or peptide-based tags to proteins, allowing their labeling and biophysical manipulation in the context of live-cell experiments (Adams et al., 2002; Keppler et al., 2004; Marks et al., 2004; Chen et al., 2005). From those techniques, we adopted the sequence-specific ligation of biotin by the *Escherichia coli* enzyme biotin ligase (BirA) for bioconjugation (Chen et al., 2005). BirA catalyzes biotinylation on a specific lysine residue within a 15-amino acid acceptor peptide (AP; Beckett et al., 1999). cDNAs encoding TfnR with the AP fused to its extracellular C terminus and an ER-retained BirA were subcloned into a bicistronic, tetracycline-regulatable adenoviral vector (Fig. 1 A). Thereby, expression levels of bTfnRs could be controlled while ensuring a high percentage of bTfnR-expressing cells (Fig. S1, A and B). For these studies we used BSC-1 cells stably expressing EGFP-tagged clathrin light chain a (LCa-EGFP) or σ2 (a subunit of the adaptor protein AP-2; σ2-EGFP), as these cells are well suited and extensively characterized for live-cell imaging (Ehrlich et al., 2004; Loerke et al., 2009; Mettlen et al., 2009, 2010). BSC-1 cells were infected with adenovirus and cultured in the presence of 5 ng/ml tetracycline, resulting in an ∼10-fold overexpression of bTfnR compared with endogenous TfnR (Fig. S1 C). When adenovirally infected cells expressing both TfnR-AP and BirA were cultured in the presence of biotin, TfnR-AP became biotinylated and trafficked normally to the cell surface (Fig. 1 B).

Surface-exposed mono-biotinylated receptors can be easily labeled with fluorescent conjugates of streptavidin, which bind tightly and specifically to biotin (Green, 1990). Importantly, because streptavidin is a tetramer it will multimerize the mono-biotinylated TfnRs. Monomeric streptavidin subunits can bind to biotin, but do so with vastly lower affinity due to a disrupted tetramer interface (Qureshi and Wong, 2002). To circumvent this problem, we generated heterotetrameric, monovalent streptavidin (SA; Fig. 1 C) by the in vitro assembly of three mutant SA subunits that can no longer bind to biotin (herein referred to as dead or D subunits) with a single wild-type/active SA subunit (referred to as A) (Howarth and Ting, 2008). The composition of various heterotetrameric SA species was confirmed by mass spectrometry, whereas their binding capacities were confirmed in vitro by using a gel-shift assay (Fig. S2). Heterotetrameric SA with one biotin-binding site (A1D3 or A1) binds biotin with nearly the same high affinity as wild-type SA (A4, 44 fM and 48 fM, respectively; Howarth et al., 2006). These reagents allowed us to label and cluster surface-biotinylated receptors in a controlled manner.

For fluorescence microscopy, SA was labeled on lysine residues using various high quantum yield Alexa Fluor (AF) dyes. When AF568 A4 or A1 (not depicted) was added to bTfnR-expressing cells and fixed after 10 min, we observed a strong colocalization with LCa-EGFP, indicating that bTfnRs were recruited into CCPs (Fig. 1 D). In previous studies using high levels of overexpression, TfnRs were diffusely distributed on the plasma membrane (Loerke et al., 2009). The punctate distribution we observed suggests that bTfnR expression under our conditions is not saturating.

Although TfnRs are generally assumed to be constitutively internalized in a ligand-independent manner, there are conflicting data (Watts, 1985; Gironès and Davis, 1989), including a recent study that suggests that it might be ligand dependent (Cao et al., 2010). Biochemical assays for monitoring CME rely on the use of modified Tfn (radiolabeled, fluorescent, or biotinylated), making it impossible to directly address whether or not Tfn itself stimulates uptake of TfnR. Therefore, to further validate our system and directly test the effect of ligand binding on TfnR internalization, we used AF647-labeled A1 and a flow cytometry assay to measure the uptake of bTfnRs in the presence or absence of Tfn. ELISA assays confirmed that A1 binding did not affect the affinity of TfnR for Tfn (unpublished data). Tfn binding had no effect on the rate of endocytic

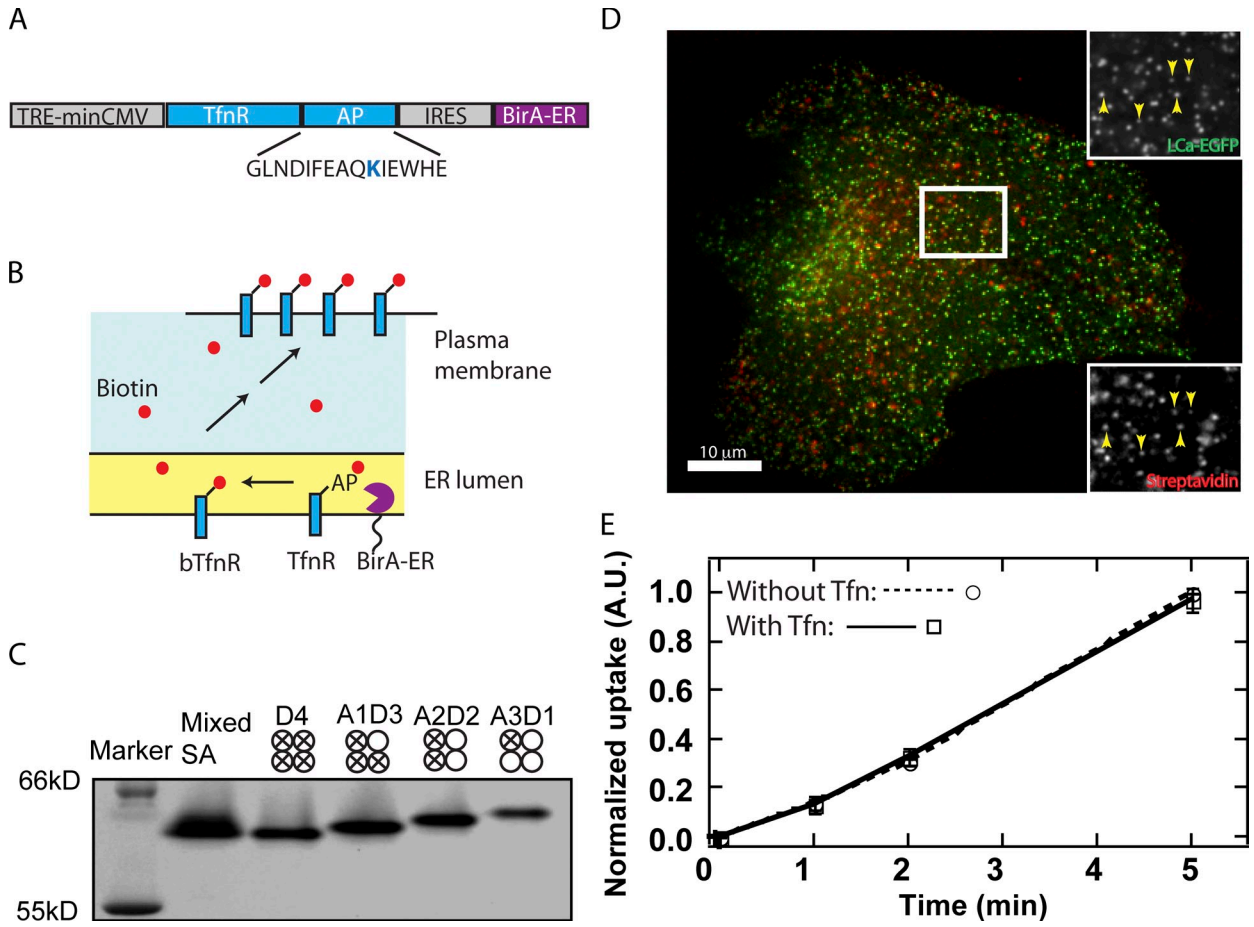

Figure 1. **Experimental system for TfnR clustering.** (A) Adenoviral bicistronic construct containing TfnR-AP and BirA-ER for tetracycline-repressible expression of bTfnRs. The Lys residue (marked in blue) within the AP is biotinylated by BirA-ER. (B) Schematic of site-specific biotinylation of TfnR. TfnRs with C-terminal acceptor peptide (AP) are biotinylated (bTfnR) by a coexpressed and ER-localized biotin ligase BirA. (C) SDS-PAGE of mixed streptavidin (SA) and purified heterotetrameric SA (eluted from a Ni-NTA column). The open circles and circles with a cross inside denote the A (active) and D (inactive/dead) monomers, respectively. (D) LCa-EGFP–expressing BSC1 cells infected with adenovirus encoding the TfnR-AP construct show colocalization of bound streptavidin with LCa-EGFP–labeled CCPs. Insets: enlarged channel separation of region highlighted by the white square indicating colocalization of streptavidin and LCa-EGFP (arrows). (E) Uptake of AF568-A1 in bTfnR-expressing cells in the presence or absence of 50 µg/ml Tfn assayed by flow cytometry (n = 4, average ± SD).

uptake of TfnR (Fig. 1 E), consistent with previous results (Watts, 1985), and demonstrating that TfnR is indeed constitutively internalized.

A4 clusters bTfnRs at the plasma membrane in living cells

Several approaches were taken to test whether A4 can cluster bTfnRs. First, cells were treated with 5 µg/ml of A1 or A4 for 10 min at 37°C. Cells were then lysed and resolved by SDS-PAGE under conditions that did not fully disrupt SA–biotin binding interactions or native TfnR dimers (Fig. 2 A). In the A1 sample, two bands were identified corresponding to monomeric and disulfide-linked dimeric bTfnR bound to A1 (Sutherland et al., 1981). After incubation with A4, in addition to the monomeric and dimeric bTfnR bound to A4, multiple slower migrating bands were detected, and these likely represent clustered bTfnR–A4 complexes. The presence of several higher molecular weight bands indicates that A4 can bind to different number of bTfnRs. The relative distribution of the A4-induced oligomeric species is shown by line scan (Fig. 2 B).

To confirm the effect of A4 on clustering bTfnR, we directly probed the spatial distribution of TfnRs on the plasma membrane using immunogold labeling of TfnRs and electron microscopy. Using an "unroofing" technique to reveal the planar ventral cell surface (Wilson et al., 2007), we observed clusters of immunogold particles in the presence of A4, but not in the presence of A1 (Fig. 2 C). Due to the large size of antibody-coupled gold particles, and hence steric hindrance, we did not expect to find gold particles in deeply invaginated CCPs. However, in thin-section electron micrographs, we clearly observed an increased clustering of TfnR in shallow CCPs in cells incubated with A4 as compared with A1 (Fig. 2 D). We quantified these observations and found a significant increase in clustering of bTfnR in CCPs in A4- compared with A1-treated cells (9.0 ± 2.3 vs. 3.3 ± 1.5 gold particles/CCP, respectively; $P < 0.001$, t test). Together, these results confirm that A4 but not A1 molecules cluster multiple TfnRs.

Further evidence for clustering of bTfnR by A4 came from examination of the relative distributions of fluorescently labeled A1 and A4 in CCPs. BSC1 cells expressing bTfnR were

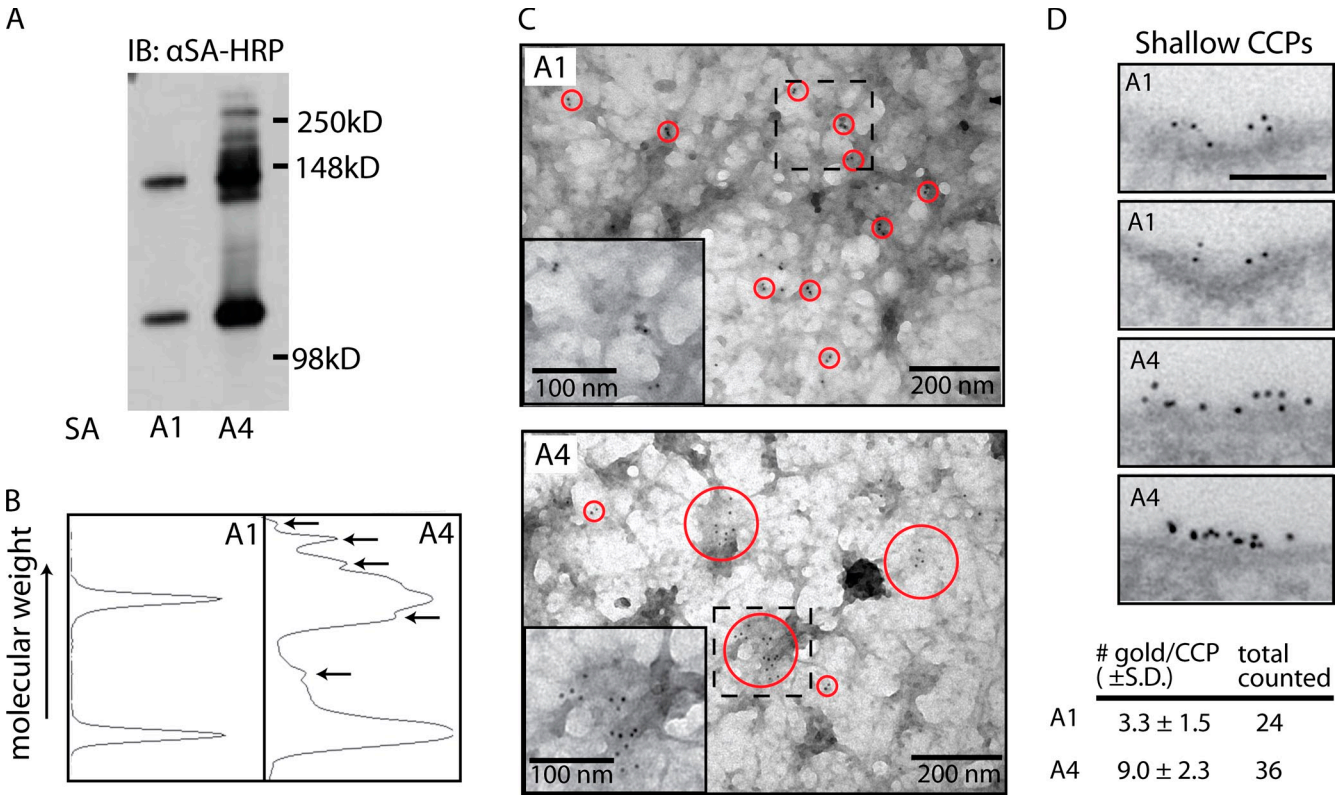

Figure 2. **Streptavidin clusters bTfnR at the plasma membrane.** (A) Immunoblot of lysates from bTfnR-expressing cells treated with either A1 or A4 for 10 min and probed with αSA-HRP to identify SA-bound bTfnR. (B) Intensity profiles of the immunoblot in A showing multiple higher molecular weight species (arrows) in A4-treated cells. (C) Electron micrographs of the ventral surface of un-roofed bTfnR-expressing cells treated with either A1 (topl) or A4 (bottom). TfnRs were labeled with D65 immunogold particles. Small circles indicate pairs of gold particles bound to TfnR dimers; large circles indicate clusters of gold particles, exclusively found in A4-treated cells. Insets: enlarged areas highlighted by the dotted squares. (D) Thin-section electron micrographs of bTfnR-expressing cells treated with either A1 (top two panels) or A4 (bottom two panels). Representative micrographs of shallow CCPs show more gold particles in CCPs in cells treated with A4, as summarized in the table.

coincubated with AF568- and AF647-labeled A1 or A4 at room temperature for 2 min to allow binding and receptor clustering into CCPs. For A1-treated cells, most detected puncta (~90%) contained both colors, whereas for A4-treated cells, there was a significantly large number of CCPs (~25%) that contained only one or the other (Fig. 3 A). We quantified the relative intensities of the two fluorophores in all CCPs that contained both. For A1-treated cells, this yielded a reasonably narrow scatter and correspondingly high correlation between the two labels (Fig. 3 B, top; $R^2 = 0.75$). In contrast, the color distributions for A4 probes are significantly more scattered (Fig. 3 B, bottom; $R^2 = 0.53$).

Assuming that both labeled versions of SA are recruited to CCPs with equal probability, and that each CCP has a particular SA capacity (N_i), we simulated the observed intensity scatter plots and correlation coefficients for A1 and A4 probes (Fig. 3 C). Importantly, we were able to accomplish this only under the additional assumption that N_i is uniformly distributed between 1 and a free parameter N_{max} (i.e., there is no preferred loading capacity). Other distributions, such as a normally distributed capacity around a preferential mean capacity, could not reproduce the experimental data (unpublished data). The uniform distribution of cargo capacity could be explained by two nonmutually exclusive models: (i) CCPs have a wide range of cargo-loading capacity, from pits with almost no loading to pits with a high loading capacity; and (ii) CCPs load a variety of other cargo molecules that compete with SA-labeled bTfnRs for space, thus resulting in a wide range of SA-loading capacity between individual CCPs. Based on the previous assumptions, we derived an analytical relationship between R^2 and N_{max} (Fig. 3 D; and see Materials and methods), from which we estimated the maximum SA capacities for A4 and A1 to be ~40 and ~80, respectively. Hence, CCPs can load up to ~80 bTfnRs with a monovalent ligand. From the lower N_{max} for A4 we conclude that this tetravalent ligand clusters bTfnRs, on average ~2 receptors per ligand. This result is in approximate agreement with our EM data (Fig. 2 D), which showed an ~2.5-fold increase in TfnR with A4-treated cells compared with A1-treated cells. Altogether, these experiments established that our method of TfnR biotinylation and ligation with streptavidin constructs of variable valency allows us to locally control the clustering of a constitutively internalized cargo molecule.

Clustering of TfnRs promotes CCP initiation

Previous studies have shown that efficient recruitment of AP-2 to model membranes requires both $PI4,5P_2$ and recognition of sorting motifs encoded in cargo molecules (Höning et al., 2005). Thus, it was surprising that overexpression of TfnR did not result in an increase in the number of CCPs, despite large cytosolic pools of AP-2 and clathrin (Loerke et al., 2009). To test

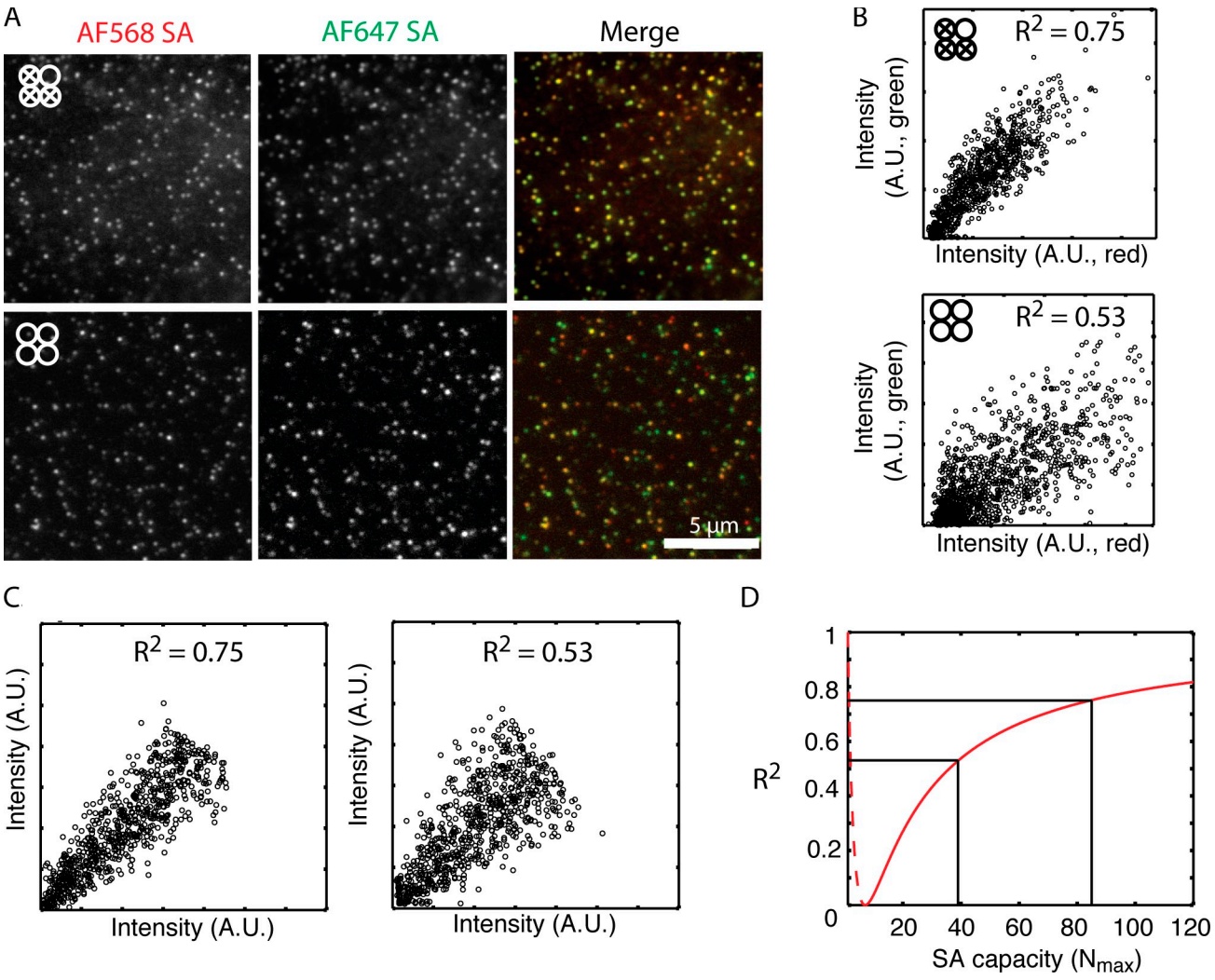

Figure 3. **Effect of clustering on the variation of cargo distribution within individual CCPs.** (A) BTfnR-expressing cells were incubated in the presence of AF568- or AF647-labeled A1 (top panels) or A4 (bottom panels). Merged images show the extent of colocalization of the differentially labeled SA ligands. (B) Representative scatter plots of the intensities in fluorescent puncta containing both A1s (top) or both A4s (bottom) from a single cell. The spread of the intensities is larger for A4 than for A1, as indicated by the square of the correlation coefficient. (C) Simulation of intensity scatter plot assuming a uniform distribution of cargo capacity and a binomial distribution of colors. (D) Theoretical estimate of maximum cargo capacity based on correlation coefficients.

whether TfnR clustering could affect the efficiency of CCP initiation in vivo, BSC1 cells expressing LCa-EGFP and bTfnR were incubated with either D4, A1, or A4 SA for 1 min at room temperature before rapid fixation, and the number of CCPs were quantified. CCPs were detected as described previously (Loerke et al., 2009) and the cell area was determined by a mask limited by the outermost CCPs. Shown in Fig. 4, A and B, are box-plots that illustrate the top and bottom quartile, the mean density of CCPs, and the full range of values obtained. As expected, because monomeric A1 does not cluster TfnR, CCP density in cells treated with A1 remained unchanged compared with cells treated with D4 (Fig. 4 A). In contrast, CCP density was significantly higher in cells incubated with A4, suggesting that TfnR clustering enhances de novo CCP formation. As differences in CCP lifetimes could affect CCP density, we also measured the initiation rate directly. CCP initiation rate as determined by live-cell total internal reflection fluorescence microscopy (TIR-FM) also increased when TfnRs were clustered (Fig. 4 B). Together, these results demonstrate that receptor clustering promotes CCP initiation.

If TfnR clustering enhances CCP initiation, then we would predict that CCPs would initiate at sites of clustered TfnR. To test this, we performed dual-channel imaging of LCa-EGFP and AF568-SA using time-lapse TIR-FM, enabling near-simultaneous visualization of CCPs and SA-bound bTfnR. We analyzed the image data by constructing characteristic intensity trajectories for all visible CCPs using previously described algorithms for CCP detection and tracking (Jaqaman et al., 2008; Loerke et al., 2009; Mettlen et al., 2010). The tracked LCa-EGFP positions were designated as the "master" channel. The signal intensity of the second, "slave" channel (AF568-SA) was then determined to produce an intensity trace of AF568-SA–bTfnR complex loading per CCP. Due to the broad distribution of CCP lifetimes, we binned CCPs into cohorts with lifetime 10–19, 20–39, 40–59, 60–79, and 80–99 s and averaged the intensity traces (Mettlen et al., 2010; Fig. 4, C and D). The monomeric

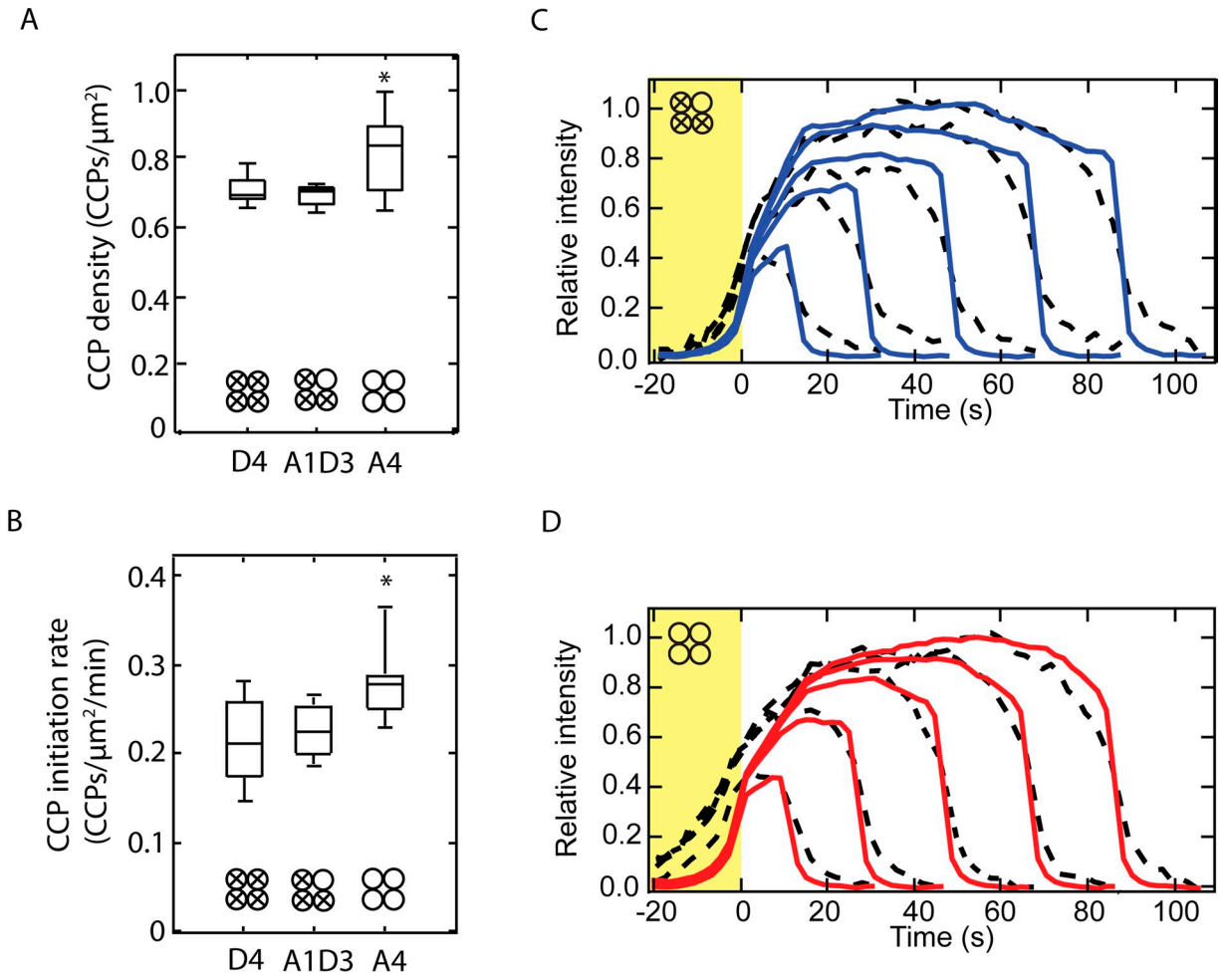

Figure 4. **CCP density increases with bTfnR clustering.** (A) Box-plot of CCP density in bTfnR-expressing cells incubated with different SAs (at least 10 regions of interest from different cells). (B) Initiation density of CCPs as determined from TIRF imaging of bTfnR-expressing cells (n = 10–16) incubated with different SAs. *, $P < 0.05$ for t test. (C) Accumulation of AF568-A1 and LCa-EGFP in A1-treated cells in five lifetime cohorts (10–19, 20–39, 40–59, 60–79, and 80–99 s) within the ensemble of CCPs. AF568A1 (dotted line) and LCa-EGFP (blue line) accumulated together (yellow region). (D) Accumulation of AF568-A4 and LCa-EGFP in A4-treated cells. AF658A4 (dotted line) was found to precede clathrin assembly (red line), as highlighted in the yellow region. A1: N_{CCP} = 28,382; N_{cell} = 5. A4: N_{CCP} = 46,508; N_{cell} = 9.

SA signal increases concomitantly with CLa-EGFP (Fig. 4 C). In contrast, the tetrameric SA signal is detected before CLa-EGFP assembly (Fig. 4 D), confirming that clustering can trigger CCP assembly.

Clustering of TfnR increases TfnR uptake

To determine if the observed increase in CCP initiation density by cargo clustering has functional ramifications with respect to the efficiency of CME, we measured cargo uptake using AF647-labeled A1 or A4 in a flow cytometry assay. The rate of A4 uptake was significantly higher compared with A1 (Fig. 5 A). These data were normalized with respect to total cell surface binding of A1 and A4 and thus cannot be explained by a simple increase in the numbers of TfnR/CCP. Internalization of AF647-labeled A1 was specific and bTfnR dependent because equimolar concentrations of unlabeled, competitive A1 or A4 decreased uptake (Fig. 5 B). As expected, addition of unlabeled D4 SA, which does not bind to biotin, did not reduce the uptake of AF647 A1 (Fig. 5 B). AF647 A1 uptake was more inhibited by unlabeled A4 than by unlabeled A1, consistent with a higher efficiency of A4 uptake.

Differential dynamic behaviors of bTfnR-containing CCPs

The higher rate of bTfnR uptake upon clustering could also be explained by increased maturation efficiency, i.e., a higher ratio of productive to abortive CCPs at the cell surface, and/or by shorter lifetimes of productive CCPs before internalization. Both parameters may depend on cargo loading into individual pits. We therefore analyzed our dual-channel time-lapse TIR-FM movies to determine the effects of cargo on CCP dynamics. SA-containing CCPs were defined as those in which the AF568-SA and LCa-EGFP signals disappear simultaneously from the TIRF field (see Materials and methods). Importantly, these averaged intensity traces represent SA content in all measured CCPs, only 36% of which contain any detectable SA signal. Therefore, to directly compare the dynamic behavior of bTfnR-containing CCPs to those that lack this cargo, we parsed them

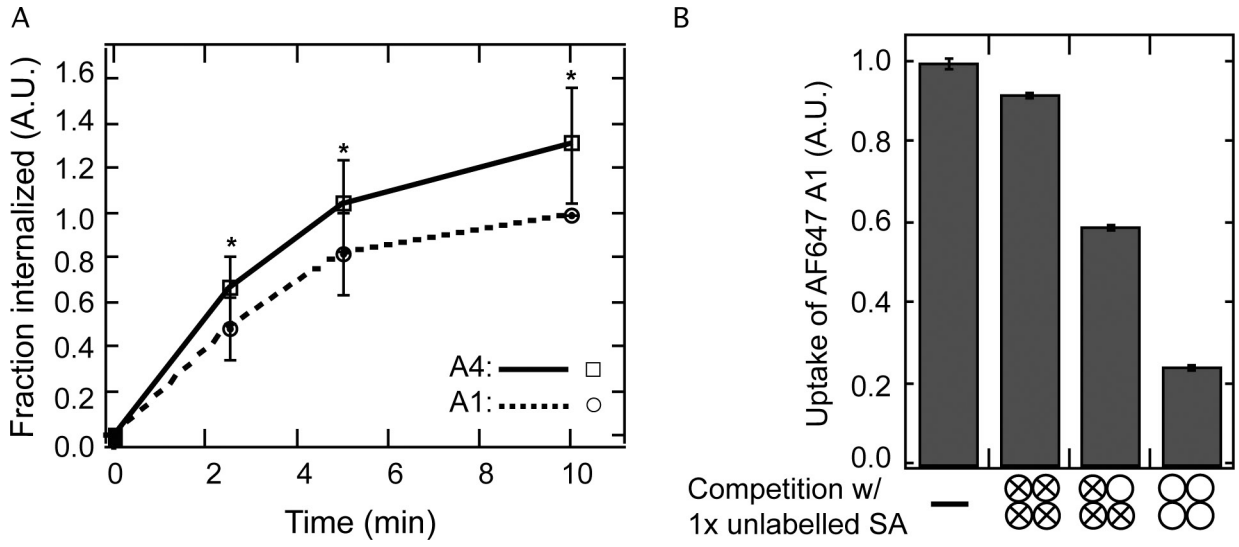

Figure 5. **Internalization of A4 is more rapid than A1.** (A) Uptake assay of AF647 A4 (blue) and A1 (red) in bTfnR-expressing LCa-EGFP BSC1 cells measured by flow cytometry ($n = 7$, average ± SD). For each experiment, the fraction internalized was normalized to the uptake of A1 at 10 min in order to compare multiple experiments. *, $P < 0.05$ by paired t test. (B) Competition of AF647 A1 uptake by the presence of different unlabeled SAs as measured by flow cytometry of 10,000 cells per condition. Error bars denote SEM.

into SA-positive or -negative CCPs (Fig. 6 A, right; and Fig. S3 A), hereafter referred to as "bTfnR-containing" or "residual" CCPs, respectively. Before the partitioning of CCPs, the intensity level of A1 in all CCPs reached 10 (Fig. 6 A, black lines). After partitioning, the intensity level of bTfnR-containing CCPs increased to 15 (Fig. 6 A, blue lines) whereas the residual CCPs exhibited near-background fluorescence levels (Fig. 6 A, dotted lines), confirming the effectiveness of the deconvolution. Of note, although the residual CCPs were not enriched in bTfnRs, they most likely contain other types of cargo.

We used this cargo-based deconvolution to examine, within the same cell, whether bTfnR-containing CCPs have distinct dynamic behaviors and if these are altered by receptor clustering. We first determined the effect of cargo clustering on CCP dynamics. Both A1 (Fig. 6 A) and A4 (Fig. S3 B) accumulated rapidly in CCPs with similar kinetics. Although the very short-lived cohort (lifetime 11–20 s) had somewhat lower average intensities, all cohorts with a lifetime >20s reached the same maximum plateau of SA intensity within the first 20 s after LCa-EGFP appearance. Thus, bTfnR loading reaches saturation early and does not appear to be a rate-limiting determinant for CCV formation.

In previous studies we used deconvolution analysis of the CCP lifetime distributions to identify three kinetically distinct populations of CCPs, including two short-lived subpopulations, termed abortive CCPs (Loerke et al., 2009). These analyses relied on combining data from 0.4 s^{-1} and 2 s^{-1} frame rate movies, to capture the full range of CCP lifetimes. Acquisition of such high sampling rates in two colors was not possible with our instrumentation. Therefore, we could not accurately identify abortive CCPs with lifetimes ≤10 s due to potentially false detections lasting up to 4 frames, nor could we distinguish robust kinetic shifts between cargo-specific CCP subsets. Nonetheless, this analysis suggested an overall lower contribution of the short-lived populations P1 and P2 for bTfnR-containing CCPs as compared with residual CCPs and longer lifetimes for the bTfnR-containing CCPs (Fig. S4).

Given the above-mentioned limitations, we instead quantified the proportion of CCPs in each lifetime cohort and compared these values for bTfnR-containing and residual CCPs. For A1–bTfnR complex-containing CCPs, the fraction of shorter-lived CCPs with lifetimes ≤20s was significantly lower (two- to threefold) than for residual CCPs in the same cell (Fig. 6 B). This was also true, albeit to a lesser extent, for A4-labeled bTfnR-containing CCPs. The decreased number of short-lived CCPs suggests that bTfnR-containing CCPs mature more efficiently (i.e., undergo fewer abortive events) compared with residual CCPs. Importantly, bTfnR-containing CCPs were identified based on the coordinated disappearance of cargo and clathrin, and thus, by definition many of the short-lived bTfnR-containing CCPs are likely to correspond to productive endocytic events, although within our temporal resolution we cannot exclude coincident coat disassembly and dispersal of surface bTfnR. Thus, the differential in short-lived abortive species between cargo-containing and residual CCPs may be even greater.

In contrast, the proportion of longer-lived species was higher for bTfnR-containing CCPs than for residual. Indeed, CCPs with lifetimes >100 s accounted for ∼25% for bTfnR complex-containing CCPs, but only ∼10% of residual CCPs. This was true for either A1- or A4-labeled cells. These data suggest that bTfnR loading prolongs CCP lifetimes. The longer lifetime of bTfnR-containing CCPs was confirmed by plotting their lifetime distributions as a survival function (Liu et al., 2009), which denotes the fraction of CCPs remaining over time. In both A1- and A4-treated cells (Fig. 6, D and E, respectively), the survival functions for bTfnR-containing CCPs were shifted to the right of the residual CCPs. Clustering bTfnR does not significantly alter the survival functions for bTfnR-containing CCPs (Fig. 6, D and E; the solid blue and red traces are not significantly different), and thus cannot account for the

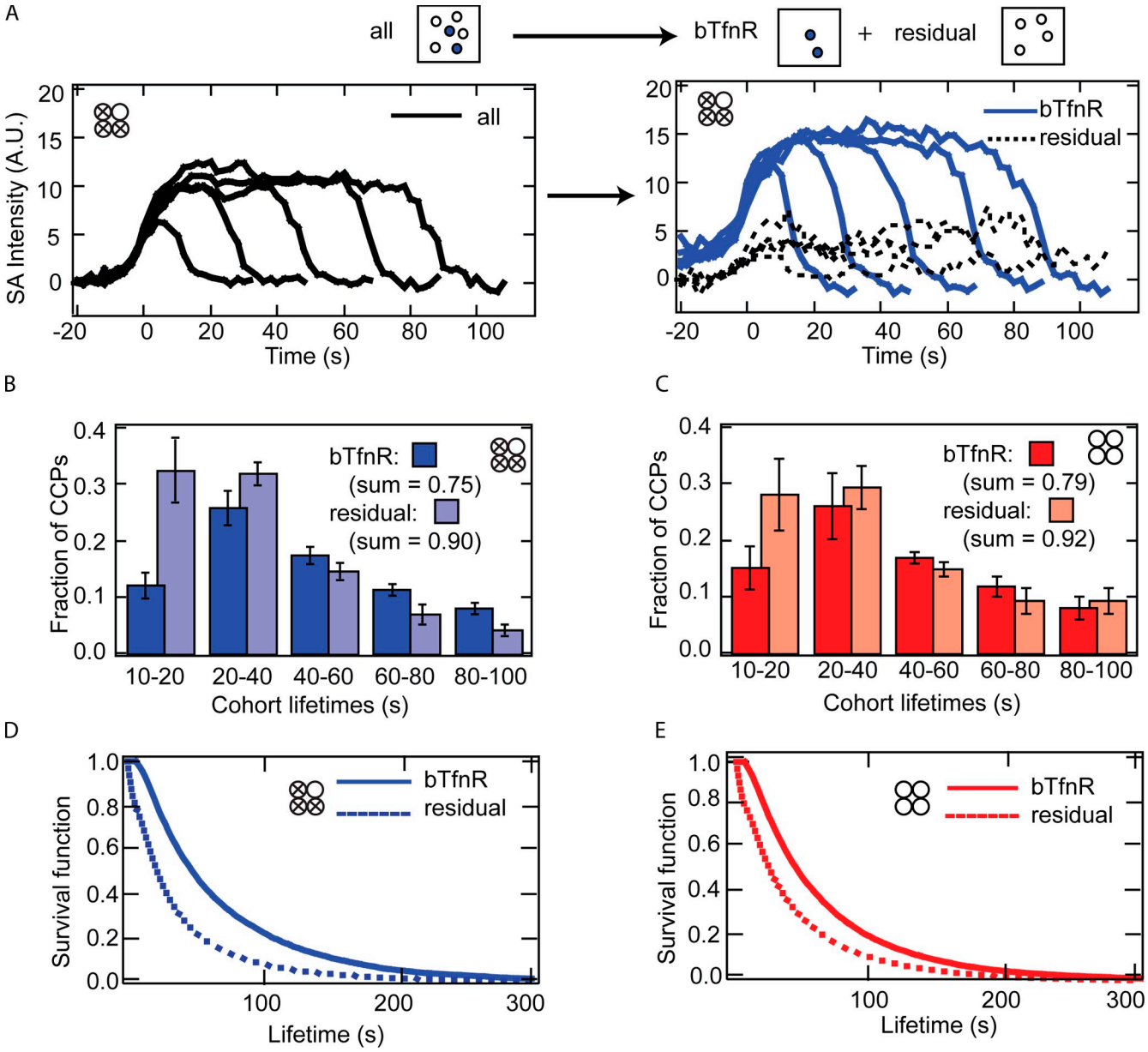

Figure 6. **Distinct dynamic behaviors of bTfnR-containing CCPs.** (A) Segregation of CCPs into bTfnR-containing and residual CCPs. (Left panel) Shown is the accumulation of AF568-A1 in five lifetime cohorts within the ensemble of EGFP-Cla–labeled CCPs. (Right panel) Cargo-based deconvolution was used to parse ensemble CCPs into either bTfnR-containing (blue) or residual CCPs (dotted). (B and C) Fraction of CCPs found in each lifetime cohort for bTfnR-containing and residual CCPs for A1- and A4-treated cells, respectively. The fraction unaccounted for in the summations are CCPs with lifetimes >100 s. All pairwise comparison CCP fractions in all lifetime cohorts were significantly different as determined by paired *t* test ($P < 0.05$), except for the 40–60-s cohort for A1-treated cells. (D and E) Survival functions of CCPs in cells expressing bTfnR and incubated with either A1 (D, blue) or A4 (E, red). BTfnR-containing and residual CCPs are shown in solid and dotted lines, respectively. A1: N_{CCP} = 28,382; N_{cell} = 5. A4: N_{CCP} = 46,508; N_{cell} = 9.

increased internalization rate of A4 vs. A1, as measured by FACS (Fig. 5 A).

bTfnR-containing CCPs are larger than residual CCPs

Finally, we asked whether the recruitment profiles of clathrin and AP-2 were affected by bTfnR clustering. We examined the intensity profiles of LCa-EGFP or σ2-EGFP for each lifetime cohort of bTfnR-containing and residual CCPs. To account for cell-to-cell variability in LCa-EGFP expression, these intensity profiles were normalized to the maximum intensity of the 80–99-s lifetime cohort of bTfnR-containing CCPs. Because the cargo-based deconvolution was performed within each cell, LCa-EGFP fluorescence intensities can be directly compared and are proportional to CCP size. In the presence of either A1 or A4, bTfnR-containing CCPs accumulate more LCa-EGFP compared with residual CCPs, irrespective of CCP lifetimes (Fig. 7, A and B). Thus, bTfnR-containing CCPs are larger than residual CCPs. Similarly, recruitment of σ2-EGFP to bTfnR-containing CCPs was higher than to residual CCPs for all cohorts (Fig. 7, C–E). We found that AP-2 was more rapidly recruited to CCPs in cells incubated with A4 compared with A1 (Fig. 7 F). Consistent

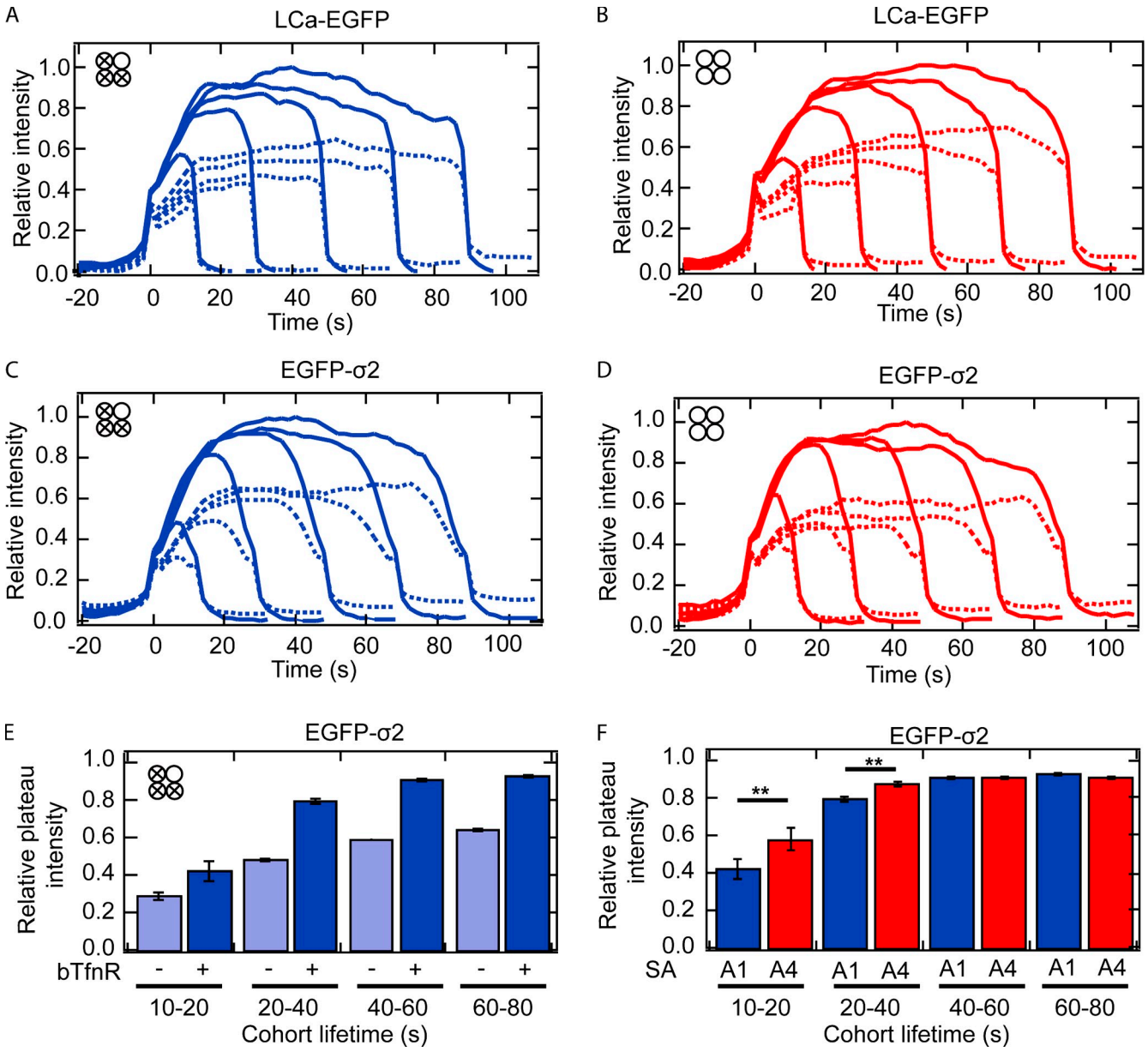

Figure 7. **BTfnR-containing CCPs recruit more AP-2 complexes and are larger than residual CCPs.** Intensity analyses based on the LCa-EGFP (A and B) or σ2-EGFP (C and D) channels in cells incubated with either A1 (A and C; blue) or A4 (B and D; red). BTfnR-containing CCPs (solid lines) were parsed out from residual CCPs (dotted lines) for five lifetime cohorts: 11–20, 21–40, 41–60, 61–80, and 81–100 s. (E) Maximum σ2-EGFP intensity plateau for each cohort (average of top five intensities ± SD) of residual (shaded blue) and bTfnR-containing (solid blue) CCPs for A1-treated cells. (F) Maximum σ2-EGFP intensity plateau of CCP cohorts in A1- (blue) and A4 (red)-containing CCPs. For LCa-EGFP, A1: N_{CCP} = 28,382; N_{cell} = 5. A4: N_{CCP} = 46,508; N_{cell} = 9. For σ2-EGFP, A1: 25,670; N_{cell} = 6. A4: 21,028; N_{cell} = 6. **, P < 0.01.

with our observation of increased CCP initiation (Fig. 4), these data demonstrate that local clustering of bTfnRs promotes the recruitment of adaptor proteins and hence CCP assembly.

Discussion

We have used a combination of biochemical assays, EM, live-cell imaging by TIR-FM, and image analysis of CCP trajectories to examine the effects of a model cargo on CCP initiation and maturation. We previously reported that gross overexpression of TfnR did not significantly affect CCP initiation or the rate of CCP maturation (Loerke et al., 2009). However, because CME is saturated under these conditions, interpretation of these data is complicated. Moreover, previous studies examined ensemble effects on CCP dynamics and did not directly analyze the behavior of cargo-containing CCPs. To overcome these limitations, we have developed new tools to manipulate cargo concentration at the single CCP level and to selectively track and analyze bTfnR-containing CCPs. This approach has allowed us to examine both the effects of specific cargo composition and loading on CCP dynamics, as well as the effect of cargo clustering on CCP dynamics.

In contrast to previous results (Loerke et al., 2009; Mettlen et al., 2010), we found that the number and rate of initial assembly

of CCPs increased upon clustering of bTfnR with tetravalent ligand. Clathrin assembly was coincident with the recruitment of monomeric ligand in nascent CCPs. In contrast, tetrameric ligand was detected before clathrin assembly, demonstrating that cargo clustering can trigger CCP initiation. Previous studies have reported that clustering and activation of signaling receptors upon ligand binding can trigger CCP initiation (Connolly et al., 1981; Puri et al., 2005); however, whether this effect is due to signaling or to receptor clustering was not clear. As TfnR is constitutively internalized, our approach effectively uncouples receptor clustering from signaling and demonstrates that cargo clustering by itself can trigger CCP initiation. This simple mechanism could perhaps explain the observation that cellular uptake of virus-like particles displaying Tfn was proportional to Tfn density (Banerjee et al., 2010).

Given that nucleation is a threshold phenomenon and efficient recruitment of AP-2 to membranes in vitro requires both cargo and PIP_2 (Höning et al., 2005), why would TfnR clustering but not its overexpression increase in CCP density/initiation rates? A simple calculation revealed that even at 100-fold overexpression, TfnR spacing would be ∼30 nm, much greater than the localized clustering that would be induced by binding 5-nm SA molecules to multiple receptors. Thus, we conclude that CCP nucleation depends heavily on the local concentration of sorting motifs. This observation is consistent with recent structural studies showing that high concentrations of cargo peptides are required to stabilize an open conformation of AP-2 for cargo and membrane binding (Jackson et al., 2010). Previous work showing that TfnR endocytosis was enhanced when a second YTRF motif was engineered into their cytoplasmic tails (Collawn et al., 1993) is also consistent with the scenario where highly localized cargo concentration stabilizes AP-2–membrane interactions and promotes CCP initiation.

By using high affinity SA to visualize bTfnR, we were able to directly compare the dynamic behavior of cargo-containing and residual CCPs. Again, in contrast to results under conditions of high overexpression (Loerke et al., 2009), we found that bTfnR-containing CCPs exhibited longer lifetimes compared with residual CCPs. Previous studies have shown that CCPs bearing ligand-activated GPCRs also exhibit increased lifetimes (Puthenveedu and von Zastrow, 2006), which again could have been a consequence of localized signaling. Here we demonstrate that constitutively internalizing cargo can also control CCP lifetimes. Neither the maturation efficiency nor the rate of CCP maturation depended on whether bTfnR was clustered (liganded by A4) or unclustered (liganded by A1). Thus, we conclude that the increased rate of endocytosis of A4 versus A1 observed by direct FACS analysis is primarily a reflection of increased rates of CCP initiation.

We and others have observed that the lifetimes of productive CCPs can vary from <30 s to >120 s (Ehrlich et al., 2004; Loerke et al., 2009). One attractive hypothesis to explain these large variations is that CCPs "wait" until they are fully loaded with cargo molecules before pinching off. However, we find that the loading of CCPs with bTfnR reaches saturation by ∼30 s, even for CCPs with lifetimes >100 s. Thus, the loading capacity is reached well before internalization of longer-lived CCPs. Moreover, clustering bTfnR with tetravalent SA, which increases the rate of cargo loading, did not affect the lifetime distribution of CCPs. From this we conclude that, at least for the constitutively internalized TfnR, cargo loading is not rate-limiting for CCP maturation.

We confirmed previous findings that cargo loading stabilizes nascent CCPs and reduces the number of abortive events (Ehrlich et al., 2004; Loerke et al., 2009); surprisingly, cargo clustering did not enhance this effect, despite the increased rate of bTfnR loading observed in the presence of tetravalent SA. However, the accelerated loading of bTfnR had the effect of partially segregating labeled bTfnR. This result can be intuitively understood if CCPs, irrespective of SA valency, have finite capacities for TfnR. As we have shown by simulation, the higher intensity variation between the two types of fluorescent bTfnR in A4-treated cells is expected as a result of fewer A4 bound to bTfnR compared with A1. Based on this result, we speculate that rapid receptor aggregation could be a mechanism to drive functional specialization of CCPs and potentially reconcile a long-standing debate as to whether and how specialized CCPs arise (Cao et al., 1998; Santini et al., 2002; Keyel et al., 2006; Puthenveedu and von Zastrow, 2006). A similar kinetic mechanism might contribute to the ligand-induced CME of GPCRs and epidermal growth factor receptors (EGFRs), which involve receptor oligomerization (Lax et al., 1991; Vidi and Watts, 2009), as well as the clathrin-dependent entry of certain viruses that involve multivalent interactions between viral proteins and their cognate receptors. Under these conditions, the acute increase of receptor–ligand complexes in nascent CCPs might exclude other CCP cargo from entering and lead to the generation of specialized CCVs for selective intracellular trafficking. CCVs enriched in signaling receptors and/or different classes of adaptors might vary in their internalization kinetics, as well as potentially being targeted to distinct populations of endosomes (Lakadamyali et al., 2006). More work will be needed to test this hypothesis.

Finally, we found that although CCPs exhibit a broad lifetime distribution, bTfnR-containing CCPs on average exhibited longer lifetimes than other CCPs within the same cell. Although we do not know the cargo composition of these residual CCPs, these data demonstrate that the cargo content can influence the rate of CCP maturation. The increased lifetimes of bTfnR-containing CCPs correlated with increased size, as measured by clathrin and AP-2 recruitment. These data extend previous findings showing cargo-specific effects on CCP dynamics, which may reflect the use of different adaptors and/or other accessory factors (Mettlen et al., 2010).

The experimental system we have used for site-specific biotinylation of TfnR coupled with the use of wild-type and heterotetrameric SA could be used to analyze the internalization kinetics of other classes of plasma membrane receptors/cargo molecules. Acute local changes in concentration, as opposed to global changes, can play an essential role in biology, especially with regard to altering the kinetics of cooperative binding during nucleation/self assembly events and in signaling (Kaizuka et al., 2009). This experimental system may prove useful for exploring these parameters in other functional contexts.

Materials and methods

Cell lines, reagents, and adenovirus infection

BSC1 monkey kidney epithelial cells stably expressing rat brain EGFP-clathrin light chain (LCa-EGFP) and EGFP sigma 2 (σ2-EGFP) were provided by Dr. T. Kirchhausen (Harvard Medical School, Boston, MA) and cultured under 5% CO_2 at 37°C in DME supplemented with 20 mM Hepes, 10 mg/ml streptomycin, 66 µg/ml penicillin, and 10% (vol/vol) fetal calf serum (HyClone). cDNA encoding the human transferrin receptor (TfnR) fused at its C terminus to the acceptor peptide (AP) was generously provided by Dr. A. Ting (Massachusetts Institute of Technology, Cambridge, MA). The TfnR-AP was placed in the tTA-regulated adenoviral vector (Altschuler et al., 1998). Biotin ligase BirA with an ER retention tag was placed in the adenoviral vector after an internal ribosomal entry site (IRES) so that TfnR-AP and BirA-ER are expressed in cis. Alexa Fluor 568– and 647–conjugated wild-type streptavidin were purchased from Invitrogen.

Cells were co-infected with tTA adenovirus and adenovirus encoding tetracycline (tet)-regulatable promoter and incubated for 18–24 h in the presence of 5 ng/ml tet before experiments. Under these conditions, bTfnR is ∼5–10 fold overexpressed compared with endogenous TfnR levels.

Purification of heterotetrameric streptavidin

E. coli expression constructs encoding His_6-tagged wild-type streptavidin (SA) and an untagged mutant harboring three-point mutations that render it unable to bind to biotin were obtained from Dr. A. Ting. Purification of heterotetrameric streptavidin (SA) was performed as described previously (Howarth and Ting, 2008). In brief, wild-type (A) and dead (D) SA monomers were expressed in *E. coli* BL21 DE3 as inclusion bodies. The His_6-tag on the "A" subunit facilitates subsequent purification. The inclusion bodies were solubilized in guanidinium hydrochloride and mixed together in a 1:3 (A:D) ratio before being diluted drop-wise into a large volume of PBS to allow refolding. Refolded mixed SA tetramers were recovered by two ammonium sulfate cuts. The mixed heterotetrameric SA were adsorbed to a Ni-NTA column and eluted sequentially with step gradients of imidazole: 25 mM (for A1D3), 50 mM (for A2D2), and 75 mM (for A3D1). Heterotetrameric SA was labeled with Alexa Fluor 568 succinimidyl ester (Invitrogen) and was estimated to have ∼3 dye molecules/protein.

Fluorescence microscopy

TIR-FM was performed on a Nikon TiE-PFS system equipped with an Apochromat 100x objective (NA 1.49), a CCD camera (Coolsnap HQ2; Photometrics), and a laser launch controlled by acousto-optic tunable filter (AOTF). Image acquisition was controlled by MetaMorph software (Universal Imaging Corp.). Cells were imaged at 37°C in a home-made imaging chamber consisting of a coverslip mounted on a slide with two strips of double-sided tape as spacer. Heterotetrameric A1 SA or WT A4 SA were diluted to 5 µg/ml in imaging media consisting of DME supplemented with 2.5% FCS and 20 mM Hepes, and added to the cells immediately before imaging. The imaging chamber was sealed with VALAP (1:1:1 of Vaseline, lanolin, and paraffin). Videos of LCa-EGFP and the SA were taken at 2-s intervals for 10 min using exposures of 100–150 ms. For fluorescence labeling, cells were fixed in 2% paraformaldehyde and 0.5% Triton for 2 min followed by another 30 min in 4% paraformaldehyde. Fixed samples were imaged on an inverted fluorescence microscope (model IX71; Olympus) using a UPLSAPO 100X NA 1.40 objective with a camera (model C4742-80-12AG; Hamamatsu Photonics) and equipped with motorized excitation and emission filter wheels (Sutter Instrument Co.). Image acquisition was controlled by the open source microscopy software Micro-Manager.

Uptake assay and flow cytometry

BTfnR-expressing LCa-EGFP BSC1 cells were detached from Petri dishes using PBS/5 mM EDTA and pelleted at 1,000 rpm for 10 min before resuspending in PBS^{4+} (PBS supplemented with 0.2 mM $CaCl_2$, 1 mg/ml BSA, 1mM EDTA, and 1 mM $MgCl_2$) at ∼3 x 10^5 cells/ml. Cells were kept on ice and Alexa Fluor 647 A1 or A4 was added to a final concentration of 5 µg/ml. Cells were transferred from ice to a 37°C water bath for the indicated amount of time, while keeping one sample on ice for the measurement of total cell surface binding. Uptake was halted by returning cells to ice and 500 µl fresh ice-cold 0.11% of Pronase solution in PBS was added to the samples (excluding the "total" sample) to digest the surface proteins for 10 min. The Pronase digestion effectively removed cell surface proteins. Cells were pelleted for 1 min at 10,000 rpm and the pellets were resuspended in 200 µl PBS, and then 200 µl of 4% paraformaldehyde was added. Samples were analyzed within 1 h using the digital LSR flow cytometer (BD). Forward scatter, side scatter, and appropriate emission were collected for 10,000 cells for each sample. Cells were gated for positive fluorescence by comparison to negative controls and percent positive was multiplied by the median of positive cells to indicate the degree of internalization. Finally, all internalization data were normalized to total surface-bound SA. Data were analyzed using FlowJo software (Tree Star, Inc.).

Data and image analysis

Custom-written software in MATLAB (The MathWorks, Inc.) for single particle tracking was used to compute trajectories from the complete inventories of CCPs imaged in live cell microscopy (Jaqaman et al., 2008). The tracking incorporates a gap-closing scheme that follows unstable signals from CCPs that either contained low amounts of fluorescent proteins or temporarily moved out of the narrow evanescent field of the TIR-FM (Loerke et al., 2009).

Intensity analysis was performed as described previously (Mettlen et al., 2010). In brief, we calculated the average intensity time courses for CCPs within a given lifetime range (i.e., CCP cohorts). The procedure first aligned and averaged the common first time point of the intensity time courses (i.e., the point at which the trajectory is first detected), yielding the "appearance-aligned" average. The time courses were then aligned to their last time point (i.e., the last detected point of the trajectory) and averaged, yielding the "disappearance-aligned" average. The global average was calculated as the weighted average of the appearance- and disappearance-aligned traces, weighted toward the appearance-aligned trace at the beginning and toward the disappearance-aligned trace at the end. The maximum plateau levels of intensity profiles were determined by averaging the five highest intensity values in each trace.

BTfnR-containing CCPs were identified based on a simultaneous decay of both the LCa-EGFP and SA signals to background levels. Specifically, a CCP was classified as bTfnR positive if the SA signal dropped to below three standard deviations above its background level during CCP disappearance (identified as described previously [Jaqaman et al., 2008; Mettlen et al., 2010]). Background levels were determined by integrating the area outside of CCPs, and both the average SA signal and the standard deviation of the background were determined through smoothing-spline fits.

Estimation of bTfnR capacity

Based on the assumptions that both labeled versions of SA are recruited to CCPs with equal probability (hence that the loading of each label follows a binomial distribution) and that the SA capacities of CCPs are uniformly distributed, the correlation coefficient can be expressed as a function of the SA maximum capacity N_{max}:

$$R^2 = \frac{(N_{\max} - 7)^2}{(N_{\max} + 5)^2} \ .$$

The correlation coefficient between two sets of values X and Y is defined as

$$R^2 = \frac{\mathrm{Cov}(X,Y)^2}{\mathrm{Var}(X)\mathrm{Var}(Y)}$$

where the expression for the variance in the case of binomially distributed values is computed as

$$\begin{aligned}\mathrm{Var}(X) &= E\{X^2\} - E\{X\}^2 \\ &= \frac{1}{N_{\max}} \sum_{n=1}^{N_{\max}} \left(\sum_{k=0}^{n} k^2 \binom{n}{k} 2^{-n} \right) - \left(\frac{1}{N_{\max}} \sum_{n=1}^{N_{\max}} \left(\sum_{k=0}^{n} k \binom{n}{k} 2^{-n} \right) \right)^2 \\ &= \frac{N_{\max}^2}{48} + \frac{N_{\max}}{8} + \frac{5}{48}\end{aligned}$$

with an analogous derivation for the covariance yielding

$$\mathrm{Cov}(X,Y) = \frac{N_{\max}^2}{48} - \frac{N_{\max}}{8} - \frac{7}{48} \ .$$

The scatter plots of Fig. 3 C were obtained by simulating 800 CCPs with uniformly distributed capacities of up to ∼80 and ∼40 for A1 and A4, respectively (corresponding to R^2 = 0.75 and R^2 = 0.53, respectively), followed by binomially distributed color assignments. The final intensities

used to generate the scatter plots were obtained by approximating the experimentally observed Poisson noise.

Electron microscopy

Anti–human TfnR monoclonal antibody HTR-D65 (against the extracellular domain) conjugated to 5.9-nm gold particles were used to label TfnR on BSC1 cells. For unroofed samples, cells expressing bTfnR were plated overnight on EM grids and treated with A1 or A4 for 2 min at room temperature before being fixed with 4% paraformaldehyde for 15 min. For thin-section samples, cells were plated on 22 × 22 glass coverslips and treated similarly as the unroofed samples. D65 immunogold particles were diluted to 2.5 µg/ml in PBS and added to the fixed cells for 60 min at room temperature. The ventral surfaces of unroofed cells were negative-stained with uranyl acetate according to published procedures (Wilson et al., 2007). Thin-section samples were processed using conventional Epon sectioning. Samples were visualized on an electron microscope (model CM-100; Philips).

Online supplemental material

Fig. S1 shows controlled expression of bTfnR from co-infection of tTa-adenovirus and adenovirus coding for TfnR-AP/BirA-ER. Fig. S2 shows mass spectrometry of purified chimeric streptavidin and gel-shift assay showing the expected streptavidin valency. Fig. S3 shows cargo-based deconvolution of A4-containing CCPs and that there is no difference between the relative plateau intensity of A1 and A4. Fig. S4 shows lifetime decomposition of A1 and A4 bTfnR-containing and residual CCPs. Online supplemental material is available at http://www.jcb.org/cgi/content/full/jcb.201008117/DC1.

We thank Alice Ting for providing the streptavidin, TfnR-AP, and BirA constructs; Vasyl Lukiyanchuk for generating the adenoviral constructs; Malcolm Wood, Director of the TSRI Core EM facility, for EM sample preparation and imaging; and Marcel Mettlen, Thomas Pucadyil, and Ya-Wen Liu for critically reading the manuscript. We also thank members of the Schmid, Danuser, and Trejo laboratories for helpful comments and Peng Zou (Massachusetts Institute of Technology) for many helpful discussions.

This work was supported by National Institutes of Health grants GM73165 (to G. Danuser and S.L. Schmid) and MH61345 (to S.L. Schmid). A.P. Liu is supported by a Leukemia and Lymphoma Society fellowship. F. Aguet is supported by a Swiss National Science Foundation fellowship. This is TSRI manuscript no. 20720.

The authors declare no competing financial interests.

Submitted: 19 August 2010
Accepted: 29 November 2010

References

Adams, S.R., R.E. Campbell, L.A. Gross, B.R. Martin, G.K. Walkup, Y. Yao, J. Llopis, and R.Y. Tsien. 2002. New biarsenical ligands and tetracysteine motifs for protein labeling in vitro and in vivo: synthesis and biological applications. *J. Am. Chem. Soc.* 124:6063–6076. doi:10.1021/ja017687n

Altschuler, Y., S.M. Barbas, L.J. Terlecky, K. Tang, S. Hardy, K.E. Mostov, and S.L. Schmid. 1998. Redundant and distinct functions for dynamin-1 and dynamin-2 isoforms. *J. Cell Biol.* 143:1871–1881. doi:10.1083/jcb.143.7.1871

Banerjee, D., A.P. Liu, N.R. Voss, S.L. Schmid, and M.G. Finn. 2010. Multivalent display and receptor-mediated endocytosis of transferrin on virus-like particles. *ChemBioChem.* 11:1273–1279. doi:10.1002/cbic.201000125

Beckett, D., E. Kovaleva, and P.J. Schatz. 1999. A minimal peptide substrate in biotin holoenzyme synthetase-catalyzed biotinylation. *Protein Sci.* 8:921–929. doi:10.1110/ps.8.4.921

Borner, G.H., M. Harbour, S. Hester, K.S. Lilley, and M.S. Robinson. 2006. Comparative proteomics of clathrin-coated vesicles. *J. Cell Biol.* 175: 571–578. doi:10.1083/jcb.200607164

Cao, T.T., R.W. Mays, and M. von Zastrow. 1998. Regulated endocytosis of G-protein-coupled receptors by a biochemically and functionally distinct subpopulation of clathrin-coated pits. *J. Biol. Chem.* 273:24592–24602. doi:10.1074/jbc.273.38.24592

Cao, H., J. Chen, E.W. Krueger, and M.A. McNiven. 2010. SRC-mediated phosphorylation of dynamin and cortactin regulates the "constitutive" endocytosis of transferrin. *Mol. Cell. Biol.* 30:781–792. doi:10.1128/MCB.00330-09

Chen, I., M. Howarth, W. Lin, and A.Y. Ting. 2005. Site-specific labeling of cell surface proteins with biophysical probes using biotin ligase. *Nat. Methods.* 2:99–104. doi:10.1038/nmeth735

Collawn, J.F., M. Stangel, L.A. Kuhn, V. Esekogwu, S.Q. Jing, I.S. Trowbridge, and J.A. Tainer. 1990. Transferrin receptor internalization sequence YXRF implicates a tight turn as the structural recognition motif for endocytosis. *Cell.* 63:1061–1072. doi:10.1016/0092-8674(90)90509-D

Collawn, J.F., A. Lai, D. Domingo, M. Fitch, S. Hatton, and I.S. Trowbridge. 1993. YTRF is the conserved internalization signal of the transferrin receptor, and a second YTRF signal at position 31-34 enhances endocytosis. *J. Biol. Chem.* 268:21686–21692.

Connolly, J.L., S.A. Green, and L.A. Greene. 1981. Pit formation and rapid changes in surface morphology of sympathetic neurons in response to nerve growth factor. *J. Cell Biol.* 90:176–180. doi:10.1083/jcb.90.1.176

Ehrlich, M., W. Boll, A. Van Oijen, R. Hariharan, K. Chandran, M.L. Nibert, and T. Kirchhausen. 2004. Endocytosis by random initiation and stabilization of clathrin-coated pits. *Cell.* 118:591–605. doi:10.1016/j.cell.2004.08.017

Gironès, N., and R.J. Davis. 1989. Comparison of the kinetics of cycling of the transferrin receptor in the presence or absence of bound diferric transferrin. *Biochem. J.* 264:35–46.

Green, N.M. 1990. Avidin and streptavidin. *Methods Enzymol.* 184:51–67. doi:10.1016/0076-6879(90)84259-J

Höning, S., D. Ricotta, M. Krauss, K. Späte, B. Spolaore, A. Motley, M. Robinson, C. Robinson, V. Haucke, and D.J. Owen. 2005. Phosphatidylinositol-(4,5)-bisphosphate regulates sorting signal recognition by the clathrin-associated adaptor complex AP2. *Mol. Cell.* 18:519–531. doi:10.1016/j.molcel.2005.04.019

Howarth, M., and A.Y. Ting. 2008. Imaging proteins in live mammalian cells with biotin ligase and monovalent streptavidin. *Nat. Protoc.* 3:534–545. doi:10.1038/nprot.2008.20

Howarth, M., D.J. Chinnapen, K. Gerrow, P.C. Dorrestein, M.R. Grandy, N.L. Kelleher, A. El-Husseini, and A.Y. Ting. 2006. A monovalent streptavidin with a single femtomolar biotin binding site. *Nat. Methods.* 3:267–273. doi:10.1038/nmeth861

Ikai, A., T. Osada, and M. Nishigai. 1988. Conformational changes of alpha-macroglobulin and ovomacroglobulin from the green turtle (*Chelonia mydas japonica*). *J. Biochem.* 103:218–224.

Jackson, L.P., B.T. Kelly, A.J. McCoy, T. Gaffry, L.C. James, B.M. Collins, S. Höning, P.R. Evans, and D.J. Owen. 2010. A large-scale conformational change couples membrane recruitment to cargo binding in the AP2 clathrin adaptor complex. *Cell.* 141:1220–1229. doi:10.1016/j.cell.2010.05.006

Jaqaman, K., D. Loerke, M. Mettlen, H. Kuwata, S. Grinstein, S.L. Schmid, and G. Danuser. 2008. Robust single-particle tracking in live-cell time-lapse sequences. *Nat. Methods.* 5:695–702. doi:10.1038/nmeth.1237

Kaizuka, Y., A.D. Douglass, S. Vardhana, M.L. Dustin, and R.D. Vale. 2009. The coreceptor CD2 uses plasma membrane microdomains to transduce signals in T cells. *J. Cell Biol.* 185:521–534. doi:10.1083/jcb.200809136

Keppler, A., H. Pick, C. Arrivoli, H. Vogel, and K. Johnsson. 2004. Labeling of fusion proteins with synthetic fluorophores in live cells. *Proc. Natl. Acad. Sci. USA.* 101:9955–9959. doi:10.1073/pnas.0401923101

Keyel, P.A., S.K. Mishra, R. Roth, J.E. Heuser, S.C. Watkins, and L.M. Traub. 2006. A single common portal for clathrin-mediated endocytosis of distinct cargo governed by cargo-selective adaptors. *Mol. Biol. Cell.* 17:4300–4317. doi:10.1091/mbc.E06-05-0421

Lakadamyali, M., M.J. Rust, and X. Zhuang. 2006. Ligands for clathrin-mediated endocytosis are differentially sorted into distinct populations of early endosomes. *Cell.* 124:997–1009. doi:10.1016/j.cell.2005.12.038

Lax, I., A.K. Mitra, C. Ravera, D.R. Hurwitz, M. Rubinstein, A. Ullrich, R.M. Stroud, and J. Schlessinger. 1991. Epidermal growth factor (EGF) induces oligomerization of soluble, extracellular, ligand-binding domain of EGF receptor. A low resolution projection structure of the ligand-binding domain. *J. Biol. Chem.* 266:13828–13833.

Liu, A.P., D. Loerke, S.L. Schmid, and G. Danuser. 2009. Global and local regulation of clathrin-coated pit dynamics detected on patterned substrates. *Biophys. J.* 97:1038–1047. doi:10.1016/j.bpj.2009.06.003

Loerke, D., M. Mettlen, D. Yarar, K. Jaqaman, H. Jaqaman, G. Danuser, and S.L. Schmid. 2009. Cargo and dynamin regulate clathrin-coated pit maturation. *PLoS Biol.* 7:e57. doi:10.1371/journal.pbio.1000057

Marks, K.M., P.D. Braun, and G.P. Nolan. 2004. A general approach for chemical labeling and rapid, spatially controlled protein inactivation. *Proc. Natl. Acad. Sci. USA.* 101:9982–9987. doi:10.1073/pnas.0401609101

Marsh, E.W., P.L. Leopold, N.L. Jones, and F.R. Maxfield. 1995. Oligomerized transferrin receptors are selectively retained by a lumenal sorting signal in a long-lived endocytic recycling compartment. *J. Cell Biol.* 129:1509–1522. doi:10.1083/jcb.129.6.1509

Mettlen, M., M. Stoeber, D. Loerke, C.N. Antonescu, G. Danuser, and S.L. Schmid. 2009. Endocytic accessory proteins are functionally distinguished by their differential effects on the maturation of clathrin-coated pits. *Mol. Biol. Cell.* 20:3251–3260. doi:10.1091/mbc.E09-03-0256

Mettlen, M., D. Loerke, D. Yarar, G. Danuser, and S.L. Schmid. 2010. Cargo- and adaptor-specific mechanisms regulate clathrin-mediated endocytosis. *J. Cell Biol.* 188:919–933. doi:10.1083/jcb.200908078

Nesterov, A., R.E. Carter, T. Sorkina, G.N. Gill, and A. Sorkin. 1999. Inhibition of the receptor-binding function of clathrin adaptor protein AP-2 by dominant-negative mutant mu2 subunit and its effects on endocytosis. *EMBO J.* 18:2489–2499. doi:10.1093/emboj/18.9.2489

Ohno, H., J. Stewart, M.C. Fournier, H. Bosshart, I. Rhee, S. Miyatake, T. Saito, A. Gallusser, T. Kirchhausen, and J.S. Bonifacino. 1995. Interaction of tyrosine-based sorting signals with clathrin-associated proteins. *Science.* 269:1872–1875. doi:10.1126/science.7569928

Puri, C., D. Tosoni, R. Comai, A. Rabellino, D. Segat, F. Caneva, P. Luzzi, P.P. Di Fiore, and C. Tacchetti. 2005. Relationships between EGFR signaling-competent and endocytosis-competent membrane microdomains. *Mol. Biol. Cell.* 16:2704–2718. doi:10.1091/mbc.E04-07-0596

Puthenveedu, M.A., and M. von Zastrow. 2006. Cargo regulates clathrin-coated pit dynamics. *Cell.* 127:113–124. doi:10.1016/j.cell.2006.08.035

Qureshi, M.H., and S.L. Wong. 2002. Design, production, and characterization of a monomeric streptavidin and its application for affinity purification of biotinylated proteins. *Protein Expr. Purif.* 25:409–415. doi:10.1016/S1046-5928(02)00021-9

Santini, F., I. Gaidarov, and J.H. Keen. 2002. G protein-coupled receptor/arrestin3 modulation of the endocytic machinery. *J. Cell Biol.* 156:665–676. doi:10.1083/jcb.200110132

Sutherland, R., D. Delia, C. Schneider, R. Newman, J. Kemshead, and M. Greaves. 1981. Ubiquitous cell-surface glycoprotein on tumor cells is proliferation-associated receptor for transferrin. *Proc. Natl. Acad. Sci. USA.* 78:4515–4519. doi:10.1073/pnas.78.7.4515

Vidi, P.A., and V.J. Watts. 2009. Fluorescent and bioluminescent protein-fragment complementation assays in the study of G protein-coupled receptor oligomerization and signaling. *Mol. Pharmacol.* 75:733–739. doi:10.1124/mol.108.053819

Warren, R.A., F.A. Green, and C.A. Enns. 1997. Saturation of the endocytic pathway for the transferrin receptor does not affect the endocytosis of the epidermal growth factor receptor. *J. Biol. Chem.* 272:2116–2121. doi:10.1074/jbc.272.4.2116

Warren, R.A., F.A. Green, P.E. Stenberg, and C.A. Enns. 1998. Distinct saturable pathways for the endocytosis of different tyrosine motifs. *J. Biol. Chem.* 273:17056–17063. doi:10.1074/jbc.273.27.17056

Watts, C. 1985. Rapid endocytosis of the transferrin receptor in the absence of bound transferrin. *J. Cell Biol.* 100:633–637. doi:10.1083/jcb.100.2.633

Wilson, B.S., J.R. Pfeiffer, M.A. Raymond-Stintz, D. Lidke, N. Andrews, J. Zhang, W. Yin, S. Steinberg, and J.M. Oliver. 2007. Exploring membrane domains using native membrane sheets and transmission electron microscopy. *Methods Mol. Biol.* 398:245–261. doi:10.1007/978-1-59745-513-8_17